Volume 1 | Number 1 | Jan 2013 | Pages 1–100

Nanoscale

www.rsc.org/nanoscale

ROYAL SOCIETY
OF CHEMISTRY

ROYAL SOCIETY
OF CHEMISTRY

www.rsc.org/nanoscale

Journal Name

COMMUNICATION

Prevention of sulfur diffusion using MoS_2-intercalated 3D-nanostructured graphite for high-performance lithium-ion batteries

Anand P. Tiwari[†1]**, HeeJoun Yoo**[†3]**, JeongTaik Lee**[2]**, Doyoung Kim**[3]**, JongHyeok Park**[2] **and Hyoyoung Lee**[*1]

We report new three-dimensional (3D)-nanostructured MoS_2-carbonaceous materials in which MoS_2 sheets are intercalated between the graphite layers that possess a multiply repeated graphite/MoS_2/graphite structure which prevents the aggregation of MoS_2 and diffusion of sulfur from carbonaceous materials, enhancing the cycling stability of Li-ion battery. We developed an efficient and scalable process applicable for mass production to synthesize non-aggregated MoS_2-intercalated 3D hybrid-nanostructured graphite based on stress induced and microwave irradiation. X-ray diffraction, X-ray photospectroscopy, Raman spectroscopy, field emission scanning electron microscopy, and high-resolution transmission electron microscopy analyses demonstrated that the as-synthesized materials consisted of MoS_2-intercalated 3D hybrid-nanostructured graphite platelets that had a multiply repeated graphite/MoS_2/graphite structure. The obtained MoS_2-graphites powder surpasses MoS_2 as an anode material in terms of specific capacity, cycle stability, and rate performances at high current densities for Li-ion batteries. The electrochemical impedance spectroscopy demonstrated that the graphite sheets not just reduced the contact resistance in the electrode but also facilitated electron transfer in the lithiation/delithiation processes. The superior electrochemical performances especially for the cycling stability of the Li-ion battery are originated from prevention of the sulfur diffusion of the MoS_2-intercalated 3D-nanostructured graphite.

Molybdenum disulfide (MoS_2) is a typical member of the transition metal dichalcogenides (TMD) family which is used in catalysis, nanotribology, and electrochemistry applications[1-3]. MoS_2 has stimulated tremendous interest in electrochemistry due to its unique electrochemical performance[4,5]. Bulk MoS_2 crystals consist of van der Waals bonded sheets of S–Mo–S layers. Each sheet, in turn, is made up of a hexagonal layer of Mo atoms between two hexagonal layers of S atoms[6,7].

Moreover, MoS_2 has a layered structure that contains galleries held together by weak van der Waals forces which provides a fast diffusion path for the movement of Li^+ ions without causing significant volume changes, making it a promising candidate for lithium-ion batteries[8-10]. MoS_2 with an enlarged interlayer distance can accommodate more Li^+ ions and lead to a high reversible capacity in initial cycling[10]. Unfortunately, in host matrixes of MoS_2, a large specific volume change commonly occurs during the cycling processes which results in pulverization of the electrodes and aggregation of electrode materials. This causes a large increase of the contact resistance and rapid capacity decay, especially under high charge and discharge current rates[11]. Therefore, the use of a suitable matrix to accommodate the volume change during the cycling processes is an efficient strategy to overcome the poor cycling and high-rate problems of MoS_2[5,12,13]. In this respect, MoS_2 sheets are uniformly dispersed in other medium such as carbonaceous materials and their aggregation can be effectively inhibited, which can lead to enhanced electrochemical properties[5,13-17]. Recently, MoS_2 and carbonaceous material hybrids have been developed[5,11-15,18,19]. However, due to the non-intimate contact between the carbonaceous materials and active materials, MoS_2 is still prone to experience strong aggregation during the cycling processes[11]. Most recently, MoS_2-graphene composites have been synthesized via hydrothermal reduction of Na_2MoO_4 and L-cysteine in the presence of graphene oxide (GO) followed by annealing under N_2[12,18,19]. Although the electrochemical performances have been improved, the yield is very low due to the possible aggregated MoS_2-graphene composites. In addition, the synthesis of MoS_2 sheets on the surface of graphene or carbonaceous materials could improve the conductivity of MoS_2, but the surface attachment of the MoS_2 sheets was not effective to prevent the aggregation of MoS_2 and the formation of polysulfides with carbon species[20]. The polysulfide clusters

can be diffused out of the carbonaceous materials. As a result, the cycling stability of the Li ion battery cell significantly decreases. Thus, until now, the MoS_2 carbonaceous composite with 2D structure is still hard to satisfy the electrochemical behavior of the lithium-ion battery[21]. Therefore, it is required to have the ideal three-dimensional (3D) nanostructure for the MoS_2 carbonaceous anode electrodes in which the MoS_2 sheets are uniformly dispersed and simultaneously intercalated between the carbonaceous materials. It is highly expected that an chemical exchange reaction of Li ions with Mo ions of the MoS_2 sheets ($MoS_2 + 4Li + 4e- \rightarrow Mo + 2Li_2S$) that are intercalated between 3D graphite structure can prevent the sulfur diffusion, eventually leading to an enhancement of cycling stability in the Li ion battery cell.

Here, we report new 3D-nanostructured of MoS_2-carbonaceous materials in which MoS_2 sheets are intercalated between the graphite layers that possess a multiply repeated graphite/MoS_2/graphite structure. The repeated graphite/MoS_2/graphite structure prevents the aggregation of MoS_2 and diffusion of sulfur from carbonaceous materials, leading to improve the cycling stability of Li-ion battery. To synthesize the hybrid 3D architectures, an induced strain and a microwave irradiation technique are used. Without using an organic solvent, this method is a facile, scalable, and efficient approach for the large-scale synthesis of graphite-backboned MoS_2 architectures. This novel method is carefully designed to yield non-aggregated MoS_2-intercalated 3D-nanostructured graphite through the direct exfoliation of graphite by using a step-by-step method including sulfur intercalation into the expanded graphite (EG) followed by metallization. We grew MoS_2 sheets on the surface of EG through a sulfur coating method on a carbonaceous surface and reaction with $MoCl_5$ as a precursor of Mo. Since sulfur is strongly attracted to carbon, sulfur can be easily coated on the carbon surface. For the uniform and facile synthesis process, we adopted a simple ball milling process and a microwave irradiation reaction. The resulting MoS_2-intercalated 3D-nanostructured graphite has continuous MoS_2-coated sheets on the EG surface doped with sulfur. The non-aggregated MoS_2-intercalated 3D-nanostructured graphite anode electrode exhibited a high specific capacity (over 800 mAh/g) and stable electrochemical performance for Li-ion battery application (up to 100 cycles).

Edge-opened graphite (EG) was obtained by acid treatment of natural graphite flakes followed by microwave treatment. Natural graphite flakes were treated with sulfuric acid and nitric acid at a ratio of 3:1 and then treated with microwaves at 700 W for 30 sec to form EG. The MoS_2-intercalated 3D-nanostructured graphite was synthesized by a simple ball milling process and a microwave irradiation technique. In a typical procedure, EG was mixed with commercially available sulfur powder at a ratio of 1:1.5 by ball milling for 24 hr to induce strain on the different layers of EG and incorporate sulfur into the different layers of EG. The resulting sulfur-coated graphite was grinded with different amounts of commercially available molybdenum chloride ($MoCl_5$) for 30 min.
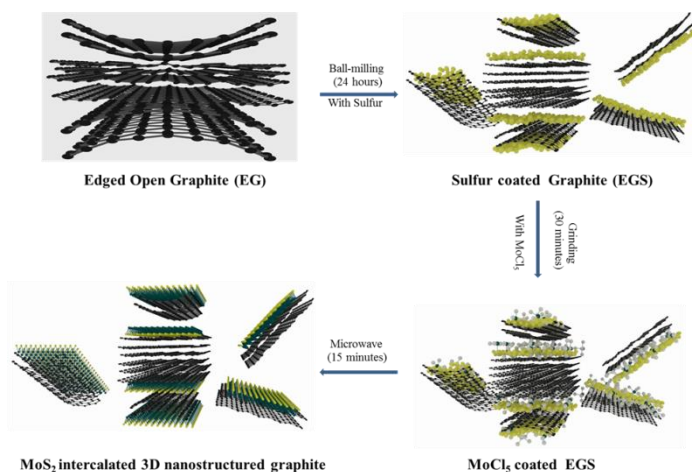

Scheme 1 Illustration of graphite-backboned MoS2-Intercalated 3D nanostructured graphite fabrication.

The final mixtures were treated with microwaves in an inert atmosphere at 700 W for 10 min to react the incorporated sulfur with $MoCl_5$ to form MoS_2. Here, two types of MoS_2-intercalated 3D-nanostructured composites were synthesized with different amounts of MoS_2 with molar mass for 0.125mmol and 0.5 mmol of $MoCl_5$ referred to as EGS-M1 and EGS-M2, respectively. The morphologies and nanostructures of the as-synthesized samples were investigated by using a field-emission scanning electron microscope (FESEM) (JEOL JMM-740F), transmission electron microscope (TEM) (JEOL JEM-2100F), powder X-ray diffractometer (XRD) (Rigaku Ultima IV), Raman Spectroscopy with laser 532 nm and X-ray photo spectroscopy (ESCA 2000, VG Microtech) for chemical compositions.

2032 coin-type cells were used for the electrochemical measurements. The working electrode slurry was composed of MoS2-intercalated 3D-nanostructured graphite as the active material, carbon black (Super P) as a conductive additive, and poly (vinylidene fluoride) (PVDF) as a binder at a weight ratio of 80:10:10 dissolved in N-methyl-2-pyrollidinone (NMP). The slurry was coated on copper foil as a current collector and dried under vacuum at 120℃ for 12 hr. All 2032 coin-type cells were assembled in an argon-filled glovebox. Lithium foil was used both as the counter and reference electrodes, and a polyethylene (PE) membrane (E16MMS, Tonen) was used as the separator. 1M LiPF6 dissolved in a mixture of ethylene carbonate (EC) and diethyl carbonate (DEC) (v/v, 1:1) (Panax Etec Co.,Ltd. Korea) was used as the electrolyte. The galvanostatic charge/discharge measurements were performed using a multichannel battery test system (WonATech, Korea) at various current densities within the voltage range of 3-0.01 V. Cyclic voltammetry (CV) and electrochemical impedance spectrometry (EIS) measurements were obtained utilizing an electrochemical analyzer (CHI 608C, CH Instrument, USA) at a scanning rate of 0.1 mVs-1 and an electrochemical workstation (Zahner Zennium, Germany) over the frequency range of 100 mHz to 100 kHz with a perturbation amplitude of 5 mV, respectively.

Scheme 1 illustrates the schematic diagram of the synthesis procedure used to produce MoS_2-intercalated 3D-nanostructured graphite via the induced stress and a microwave irradiation technique. The interaction between a sulfur molecule and the graphite surface is stronger than the van der Waals force between graphite sheets due to their similar electro-negativity values[20,21]. However, mass production of high-quality sulfur-coated graphite was obtained by using ball milling for 24 hr. Sulfur is a moderately sticky material for the graphite plane, which remains on the surface of graphite while grinding with $MoCl_5$. The reaction between sulfur and $MoCl_5$ occurs when the grinded mixture is treated with microwaves for 10 min and finally, MoS_2 is formed on the surface of graphite. The reaction to form MoS_2 can be described as[22]

$$2MoCl_5 + 14S \rightarrow 2MoS_2 + 5Cl_2S_2$$
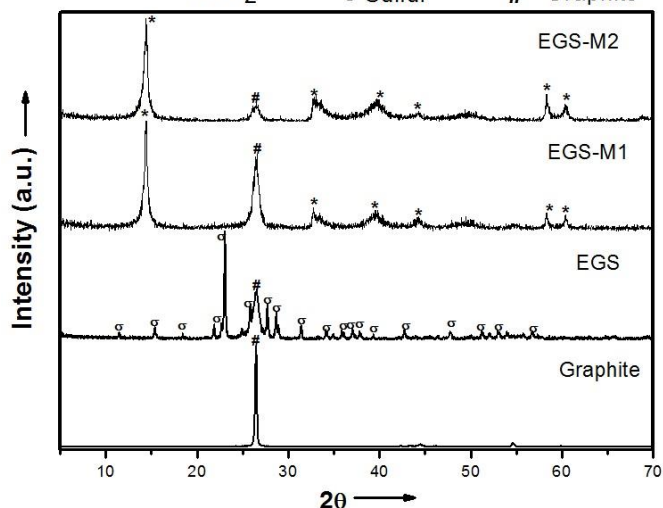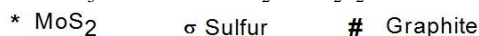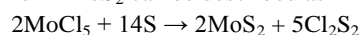
Figure 1 XRD patterns of Graphite, Sulfur intercalated expanded graphite (EGS), and MoS2-Intercalated 3D nanostructured graphite composites EGS-M1 and EGS-M2.

The MoS_2-intercalated 3D-nanostructured graphite samples were firstly confirmed by X-ray diffraction (XRD) patterns. The XRD patterns of the MoS_2-intercalated 3D-nanostructured graphite samples are shown in Figure 1. The XRD pattern is indexed as hexagonal 2H-MoS_2 (JCPDS 6-97). The single strong (002) reflection at $2\Theta = 14.20$, corresponding to a d-spacing of 0.615 nm, reveals a well stacked layered structure for both EGS-M1 and EGS-M2. This shows that microwave treatment is sufficient to obtain good crystallinity of MoS_2. Moreover, the diffraction peaks of the EGS-M1 and EGS-M2 samples at $2\Theta = 33.50, 39.60$, and 59.10 correspond to the (100), (103), and (110) planes of MoS_2, respectively. As observed in the XRD patterns of EGS-M1 and EGS-M2 shown in Figure 1, it is clear that sulfur peaks are not present whereas they are present in the sulfur intercalated expanded graphite sample, revealing that the microwave treatment for 10 min is sufficient to form well stacked MoS_2 layers from $MoCl_5$. The broad reflection at $2\Theta = 26.40$ originates from the expanded graphite. It is clear from the XRD pattern, the (002) peak of expended graphite is shifted to lower angle in EGS-M1 and EGS-M$_2$ samples, compared with graphite sample, due to

intercalation of MoS_2 between the expanded graphite sheets. Also the interlayer distances between graphite sheets are changed from 3.33 Å to 3.85 Å in graphite to MoS_2 intercalated expanded graphite sample. Moreover in X-ray photospectroscopy (XPS) measurements (Supplementary Figure S1) we did not observe chlorine peaks in XPS measurement, which implies that 10 min microwave treatment is sufficient for the reaction between $MoCl_5$ and sulfur to form MoS_2 sheets.
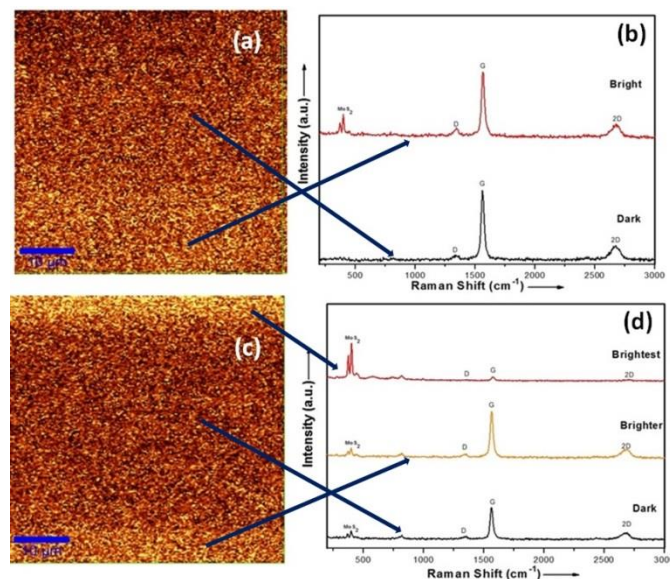

Figure 2 Raman Characterizations: (a) and (b) Raman Mapping and corresponding spectra of EGS-M1, (c) and (d) Raman Mapping and corresponding spectra of EGS-M2.

Raman spectroscopy is used to confirm the intercalation of MoS_2 sheets between the graphite layers by Raman mapping. Figures 2(a) and (c) show the Raman mapping and Figures 2(c) and (d) show the corresponding Raman spectra of the composites EGS-M1 and EGS-M2, respectively. The corresponding spectra of the sample EGS-M1 show that the bright part contains both MoS_2 and graphite peaks, but the dark part contains only graphite peaks. The D and G peak ratio of the bright part spectra is increased, which reveals that MoS_2 sheets are intercalated between the graphite layers. However, the corresponding spectra of the sample EGS-M2 exhibit that most of the MoS_2 sheets are grown on the surface of graphite sheets due to higher amount of MoS_2. The bright part of the Raman spectra shows that only MoS_2 peaks with very low intensity of G peak and D peak disappears, which implies that the MoS_2 sheets are not intercalated between graphite sheets at that part. Moreover less, bright spectra has MoS_2 peaks as well as the higher ratio of D and G peaks in comparison with the dark part, which implies that the less bright part contains an intercalation of MoS_2 between the graphite sheets.

The nanostructures of the as-prepared MoS_2-intercalated 3D-nanostructured graphite samples were examined in detail by HRTEM. It can be clearly seen that MoS_2 sheets are well supported on the graphite sheets during microwave irradiation. The overlapping of MoS_2 sheets on graphite is important when using the poorer conducting MoS_2 as an electrode material. It is

revealed in Figures 3(a) and 3(b) that MoS_2 has a well layered structure with d(002) = 0.61 nm, which agrees with the XRD analysis results. It can be clearly seen that in EGS-M1 sample (Figure 3(a)), MoS_2 sheets are well intercalated between the graphite layers but in EGS-M2 sample (Figure 3(b)), most of MoS_2 sheets grow on the surface of graphite which agrees with the Raman mapping (Figure 2). The repeated 3D nanostructured of EGS-M1 sample is also investigated by HRTEM analysis (Supplementary Figure S2).
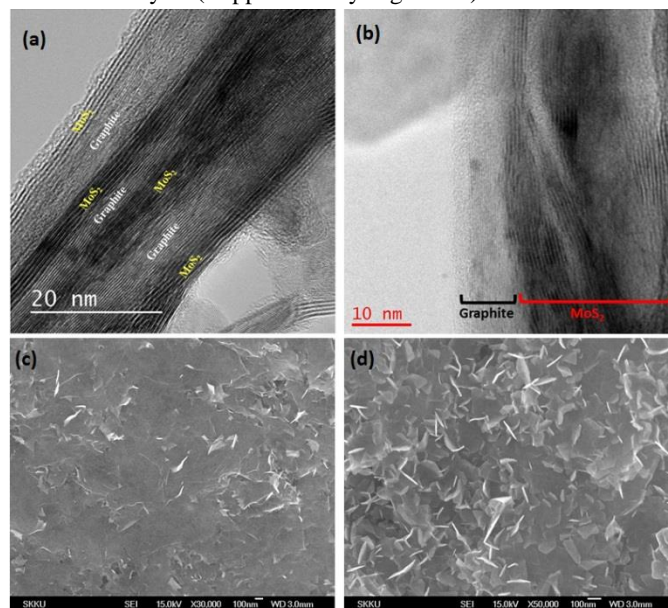

Figure 3 Nanostructures of MoS_2-intercalated 3D nanostructured graphite: (a) and (b) HRTEM images of EGS-M1 and EGS-M2, respectively. (C) and (d) SEM images of EGS-M1 & EGS-M2, respectively.

Figures 3(c) and 3(d) are SEM images of the as-synthesized EGS-M1 and EGS-M2 samples, respectively. Due to the strong electronegativity between carbon and sulfur, sulfur maintained its covered morphology (Supplementary Figure S4) on the expanded graphite during the microwave irradiation reaction and reacted with $MoCl_5$. Therefore, the MoS_2 layer structure is grown up between the surfaces of the expanded graphite. Isolated MoS_2 was not observed in both nanostructures, which demonstrates that MoS_2 sheets are well supported on the graphite surface. However, due to the higher amount of MoS_2 in EGS-M2 sample, the MoS_2 sheets grow perpendicular to the surface of graphite sheets as shown in Figure 3(d). It is also noted that the MoS_2 sheets show arc-like shapes with thinner sides and thicker middles while most of the sheets are in tight contact with each other, which helps them to grow vertically on the surface of the graphite sheets. Moreover, MoS_2 sheets are flat on the graphite surfaces in EGS-M1 as shown in Figure 3(c).

The amount of MoS_2 in EGS-1 and EGS-M2 samples are calculated by (Thermo gravimetric analysis) TGA. It is found that EGS-1 and EGS-M2 samples contain 5.43 wt% and 13.87 wt% of MoS_2 respectively (Supplementary Figure S3).

The electrochemical performances were investigated by cyclic voltammetry (CV) and galvanostatic charging-

discharging cycling. Figures 4(a) and (b) show voltammograms of the first five cycles of EGS-M1 and EGS-M2, respectively. The as-synthesized EGS-M1 sample shows two reduction peaks at 1.15 and 0.55 V in the first cathodic sweep, as shown in Figure 5(a). The peak at 0.55 V is attributed to the conversion reaction process[23-25].

$$MoS_2 + 4Li + 4e^- \rightarrow Mo + 2Li_2S$$
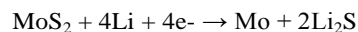
The peak at 0.9 V can be attributed to the coordination of Mo by six S atoms (MoS_6), which changes from trigonal prisms to octahedral in the MoS_2 structure along with the intercalation of lithium in MoS_2[26]. These reduction peaks disappear from the second cycle because of the decomposition of MoS_x into Mo nanoparticles embedded in the Li_2S matrix through the conversion reaction. Interestingly, as a previous result obtained with carbon and the MoS_2 composite, the reduction peaks for the conversion reaction of MoS_2 at the first cycle always appeared below ~0.9 V and ~ 0.5 V. However, the first reduction peaks of EGS-M1 in this analysis were at 1.15 and 0.55 V. This is important evidence for the MoS_2 coating structure on graphite. Due to the close coating structure between the MoS_2 layer and graphite, the conversion reaction of MoSx during the reduction potential is facilitated. On the other hand, the reduction peaks of EGS-M2 occurred at 0.45 and 1.05 V in the first cathodic sweep, which is a lower reduction potential than EGS-M1 as shown in Figure 4(b). This is due to the not closely covered MoS2 layer of EGS-M2, which is different from EGS-M1 (Figures 3 (c) and (d)). Slight shifts of the reduction peak potentials of EGS-M1 and EGS-M2 compared to the MoS2 electrode can be caused by overlap of the electrochemical lithium storage of MoS_2 and graphite sheets[5].
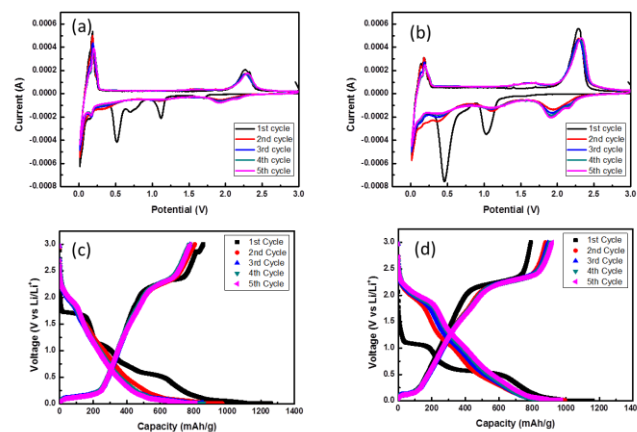
Figure 4 Electrochemical performances of MoS_2-intercalated 3D nanostructured graphite: (a) and (b) the first five cycles cyclic voltammograms of EGS-M1 and EGS-M2, respectively. (c) and (d) representative charge-discharge curve of EGS-M1 and EGS-M2 at current density 50mA/g, respectively.

In addition, the peaks below ~0.2 V during the cathodic sweep of both samples are due to the intercalation of lithium ions into the graphite sheets and the transformations between different stages of the intercalation compounds[27]. The 2nd, 3rd, 4th, and 5th cathodic sweeps of the EGS-M1 and EGS-M2 electrodes showed two reduction peaks at 1.10 and 1.80 V but

the peaks which were present in first cathodic sweep of both composites disappeared, which agrees with the previously reported lithiation and delithiation profiles[12]. While the oxidation peak during the reverse anodic sweep of EGS-M1 and EGS-M2 concerning the delithiation profiles of LiS_2 appeared at 2.25 V, the oxidation peaks of MoS_2 appeared at 2.4 V and in the case of carbon and the MoS_2 composite, it appeared around 2.3V. In this work, the oxidation reaction of LiS_2 on the MoS_2-coated graphite sample is also facilitated, resulting in the oxidation peak at a lower anodic potential. This feature also agrees with a previous report involving MoS_2-coated MWCNTs[15].

Figures 4(c) and 4(d) show the first five discharge-charge profiles of the EGS-M1 and EGS-M2 samples at a current density of 50 mA/g, respectively. Figure 4(d) exhibits three potential plateaus at 1.10 V, 0.6 V, and 0.2 V for the EGS-M2 electrodes in the first discharge process, which agree with the CV measurements. The plateau at 1.10 V confirms that formation of $LixMoS_2$ and the plateau at 0.6 V suggests the conversion reaction in which MoS_2 is decomposed into Mo particles embedded in a Li2S matrix[5,12,28]. However, the plateau at the potential of 0.2 V demonstrates lithium deintercalation from the graphite sheets[27]. The slope potential beyond 0.6 V indicates the formation of a gel-like polymeric layer from electrochemical driven electrolyte degradation. However, the 2nd, 3rd, 4th, and 5th discharge curves of the EGS-M2 electrode shows plateaus at 1.9 V, 1.2 V, and below 0.2 V, which is consistent with its CV after the 1st scan. The charge process of the EGS-M2 electrode displays two conspicuous potential plateaus at 0.20 V and 2.20 V due to the high crystallinity of MoS_2 and lithium intercalation in the graphite sheets. Moreover, we observed potential plateaus at 1.70 V, 1.10 V, 0.6 V, and below 0.2 V in the first discharge process of EGS-M1, as shown in Figure 4(c). The extra plateau at a potential of 1.70 V may be due to the high crystallinity and high amount of graphite sheets in EGS-M2. Figures 4(c) and 4(d) illustrate that the initial discharge capacities of the EGS-M1 and EGS-M2 electrodes are 1,260 and 1,190 mAh/g, respectively, while the initial reversible charge capacities are 850 and 890 mAh/g, respectively. The irreversibility in the first cycles is due to the formation of a solid electrolyte interface (SEI) film as well as decomposition of electrolyte and reduction of oxygen-containing groups. Both samples exhibited a higher specific capacity than the theoretical capacity of bulk MoS_2 (167 mAh/g)[29].

Figure 5(b) shows the cyclic stability of the EGS-M1 and EGS-M2 composite electrodes at a constant current density of 50 mA/g. The reversible charge capacity of the EGS-M2 electrode decreased from 1,020 to 490 mAh/g after 100 cycles as shown in Figure 5(b), while the EGS-M1 electrode exhibited an excellent cyclic stability even over 100 cycles. The reversible charge capacity of the EGS-M1 electrode slightly increased. After 100 cycles, the reversible charge capacity of the EGS-M1 electrode remained at 810 mAh/g. Thus, the
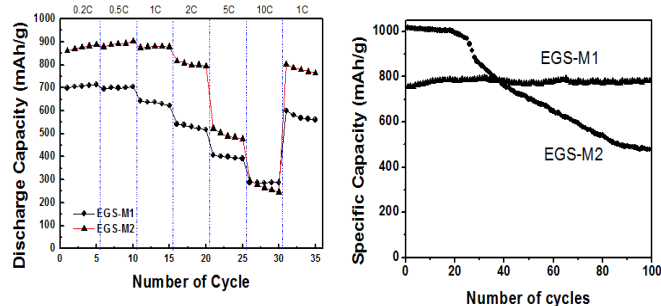
Figure 5 (a) Rate capability of EGS-M1 and EGS-M2 at different current densities, (b) Cycling behavior of EGS-M1 and EGS-M2 at a current density 50mA/g.

graphite sheets not only enhanced the specific capacity of the composites, but also improved the cyclic stabilities of the MoS_2-intercalated 3D-nanostructured graphite due to homogeneous dispersion and intercalation of MoS_2 sheets between the extended graphite layers. Moreover, the excess amount of MoS_2 in the EGS-M2 composite decreased its cyclic stability because MoS_2 layers which grow perpendicular on the surface of graphite sheets gradually curl up and agglomerate during cycling (Supplementary Information Figure S5). Figure 5(a) illustrates the rate performances of the EGS-M1 and EGS-M2 composite electrodes where both EGS-M1 and EGS-M2 electrodes exhibited good high-rate performances. Reversible capacities of 310 mAh/g and 290 mAh/g were achieved at a 10 C rate for the EGS-M1 and EGS-M2 electrodes, respectively. These results are significantly higher than those of previously reported MoS_2 electrodes.

Electrochemical impedance spectrometry (EIS) measurements were performed after 10 cycles in order to better understand the electrochemical performances of the EGS-M1 and EGS-M2 electrodes. Supplementary Figure S6 (a) shows the Nyquist plots of the EGS-M1 and EGS-M2 electrodes. The equivalent circuit model for the impedance response is shown in Supplementary Figure S6 (b)[12] where R_e represents the internal resistance, R_f and CPE1 are the resistance and constant phase element of the SEI, respectively, R_{ct} and CPE2 are the charge-transfer resistance and constant phase element of the electrode/electrolyte interface, respectively, and Z_w is the Warburg impedance corresponding to the lithium diffusion process. The high frequency semicircle in Supplementary Figure S6 (a) corresponds to the resistance, R_f, and CPE1 of the SEI film. Meanwhile, the medium frequency semicircle can be attributed to the charge-transfer resistance, R_{ct}, and CPE2 of the electrode/electrolyte interface whereas the inclined line in the low frequency region corresponds to lithium diffusion processes. The R_f and R_{ct} values were obtained by modeling ac impedance spectra based on a modified equivalent circuit[30]. The R_f and R_{ct} values of the EGS-M1 electrode are 11.38 Ω and 63.07 Ω, respectively, which are lower than those of the EGS-M2 electrode, which were 14.69 Ω and 91.30 Ω, respectively. The contact resistance and charge transfer of the Li^+ insertion/extraction of EGS-M1 are lower than those of the EGS-M2 electrode because MoS_2 grows vertically and curls during cycling in the EGS-M2 electrode (Figure 3(d)), which

reduces the electron transfer and also the extraction of Li ions from the LiMoS$_2$ structure[31]. On the other hand, the R$_f$ and R$_{ct}$ values of the EGS-M1 electrode are lower than those of previously reported MoS$_2$ electrodes, which confirm that the graphite layers preserve the improved conductivity and enhance the rapid electron transport during the Li ion insertion/extraction reaction[5].

A facile process for new 3D-nanostructured of MoS$_2$-carbonaceous materials in which MoS$_2$ sheets are intercalated between the expanded graphite layers was developed for the high cyclic stability of Li-ion batteries. Characterization of the nanostructure by XRD, XPS, raman spectroscopy, TEM, and FESEM demonstrated that the layered MoS$_2$ was supported on the graphite surface, forming MoS$_2$-intercalated 3D-nanostructured graphite. The electrochemical evaluations revealed that the EGS-M1 and EGS-M2 electrodes have higher specific capacities than previously reported MoS$_2$ electrodes. In particular, the EGS-M1 electrode in which MoS$_2$ sheets are perfectly intercalated between the graphite layers demonstrated much better cyclic and rate performances. The excellent electrochemical performances can be attributed to the synergetic interaction between MoS$_2$ and graphite. Therefore, the present study suggests that newly developed MoS$_2$-intercalated 3D nanostructured graphite can produce very versatile anode materials for Li-ion batteries suitable for large-scale production.

Notes and references

1. Centre for Integrated Nanostructure Physics (CINAP), Institute of Basic Science (IBS), Department of Chemistry, Sungkyunkwan University, 300 Cheoncheon-Dong, Jangan-Gu, Suwon, Gyeonggi-Do 440-746, South Korea Email: hyoyoung@skku.edu; Fax: (+) 82-31-299-5934; Tel: (+) 82-31-299-4566;

2 Department of Chemical and Biomolecular Engineering, Yonsei University, 50 Yonsei-ro, Seodaemun-gu, Seoul 120-749, Republic of Korea

3 Department of Energy Science, Sungkyunkwan University, 2066 Seoburo, Jangan-gu, Suwon, Gyeonggi-do 440-746, Republic of Korea

† Equally contributed

Electronic supplementary information (ESI) available

1   A. Nogueira, R. Znaiguia, D.Uzio, P. Afanasiev, G. Berhault, *Appl. Catal., A*, 2012, **92**, 429-430.

2   L. Rapoport, *Nature*, 1997, **387**, 791-793.

3   X. L. Li, Y. D. Li, *J. Phys. Chem. B*, 2004, **108**, 13893-13900.

4   X. P. Fang, X. Q. Yu, S. F. Liao, Y. F. Shi, Y. S. Hu, Z. X. Wang, G. D. Stucky, L. Q. Chen, *Microporous Mesoporous Mater.,* 2012, **151**, 418-423.

5   Z. Wang, T. Chen, W. Chen, K. Chang, L. Ma, G. Huang, D. Chen, J. Y. Lee, *J. Mater. Chem. A*, 2013, **1**, 2202-2210.

6   R. Tenne, L. Margulis, M. Genut, G. Hodes, *Nature*, 1992, **360**, 444-446.

7   H. S. S. R. Matte, A. Gomathi, A. K. Manna, D. J. Late, R. Datta, S. K. Pati, C. N. R. Rao, *Angew. Chem.*, 2010, **49**, 4059-4062.

8   H. Hwang, H. Kim, J. Cho, *Nano Lett.*, 2011, **11**, 4826-4830.

9   S. J. Ding, D. Y. Zhang, J. S. Chen, X. W. Lou, *Nanoscale*, 2012, **4**, 95-98.

10   G. D. Du, Z. P. Guo, S. Q. Wang, R. Zeng, Z. X. Chen, H. K. Liu, *Chem. Commun.*, 2009, **46**, 1106-1108.

11   Y. Gong, S. Yang, Z. Liu, L. Ma, R. Vajtai, P. M. Ajayan, *Adv. Mater.* 2013, **25**, 3979-3984.

12   K. Chang, W. Chen, *ACS Nano,* 2011, **5**, 4720-4728.

13   K. Chang , W. X. Chen , *J. Mater. Chem.* 2011, **21**, 17175-17184.

14   Q. Zhang, K. Yu, B. Zhao, Y. Wang, C. Song, S. Li, H. Yin, Z. Zhang, Z. Zhu, *RSC Advances,* 2013, **3**, 10994-11000.

15   Y. Shi, Y. Wang, J. I. Wong, A. Y. S. Tan, C. Hsu, L. Li, Y. Lu , H. Y. Yang, *Sci. Reports,* 2013, **3**, 2169.

16   A. K. Geim, K. S. Novoselov, *Nat.Mater.*, 2007, **6**, 183-191.

17   E. Yoo, J. Kim, E. Hosono, H. S. Zhou, I. Honma, *Nano Lett.*, 2008, **8**, 2277-2282.

18   X. Cao, Y. Shi, W. Shi, X. Rui, Q. Yan, J. Kong, H. Zhang, *Small*, 2013, **9**, 3433-3438.

19   G. Huang, T. Chen, W. Chen, Z. Wang, K. Chang, L. Ma, F. Huang, D. Chen, J. Y. Lee, *Small,* 2013, **9**, 3693-3703.

20   T. Lin, Y. Tang, Y. Wang, H. Bi, Z. Liu, F. Huang, X. Xie, M, Jiang, *Energy Environ. Sci.,* 2013, **6**, 1283–1290.

21   J. Xu, J. Shui, J. Wang, M. Wang, H. Liu, S. Dou, I. Jeon, J. Seo, J. Baek, L. Dai, *ACS Nano,* 2014, **8**, 10920–10930.

22   H. Yoo, A. P. Tiwari, J. Lee, D. Kim, J. Park and Hyoyoung Lee, *Nanoscale, 2015,* **7**, 3404-3409.

23   K. Chang, W. Chen, L. Ma, H. Li, H. Li, F. Huang, Z. Xu, Q. Zhang, J. Y. Lee, *J. Mater. Chem.*, 2011, **21**, 6251-6257.

24   G. X. Wang, S. Bewlay, J. Yao, H. K. Liu, S. K. Dou, *Electrochem. Solid-State Lett.* 2004, **7**, A321-A323.

25   Y. MiKi, D. NakazatoIkuta, H. Ikuta, T. Uchida, M. Wakihara, *J. Power Sources,* 1995, **54**, 508-510.

26   S. J. Ding, J. S. Chen, X. W. Lou, *Chem. Eur. J.*, 2011, **17**, 13142-13145.

27   M. Yoshio, H. Wang, K. Fukuda, Y. Hara, Y. Adachic, *J. Electrochemical Society,* 2000, **147**, 1245-1250.

28   R. Dominko, D. Arcon, A. Mrzel, A. Zorko, P. Cevc, P. Venturini, M. Gaberscek, M. Remskar, D. Mihailovic, *Adv. Mater.,* 2002, **14**, 1531-1533.

29   J. Xiao, D. W. Choi, L. Cosimbescu, P. Koech, J. Liu, J. P. Lemmon, *Chem. Mater.*, 2010, **22**, 4522-4524.

30   S. B. Yang, X. L. Feng, L. J. Zhi, Q. A. Cao, J. Maier, K. Mullen, *Adv. Mater.* 2010, **22**, 838-842.

31   X. B. Chen, J. H. He, D. Srivastava, J. Li, *Appl. Phys. Lett.,* 2012, **100**, 263901.

Nanoscale Accepted Manuscript